Low-Frequency Variability of Surface Air Temperature in a 1000-Year Integration of a Coupled Atmosphere–Ocean–Land Surface Model

SYUKURO MANABE AND RONALD J. STOUFFER

Geophysical Fluid Dynamics Laboratory/NOAA, Princeton University, Princeton, New Jersey

(Manuscript received 28 February 1995, in final form 18 July 1995)

ABSTRACT

This study analyzes the variability of surface air temperature (SAT) and sea surface temperature (SST) obtained from a 1000-yr integration of a coupled atmosphere–ocean–land surface model, which consists of general circulation models of the atmosphere and oceans and a heat and water budget model of land surface.

It also explores the role of oceans in maintaining the variability of SAT by comparing the long-term integration of the coupled model with those of two simpler models. They are 1) a "mixed layer model," that is, the general circulation model of the atmosphere combined with a simple slab model of the mixed layer ocean, and 2) a "fixed SST model," that is, the same atmosphere model overlying seasonally varying, prescribed SST.

With the exception of the tropical Pacific, both the coupled and mixed layer models are capable of approximately simulating the standard deviations of observed annual and 5-yr-mean anomalies of local SAT. The standard deviation tends to be larger over continents than over oceans, in agreement with the observations. Over most continental regions, the standard deviations of annual, 5-yr- and 25-yr-mean SATs in the fixed SST model are slightly less than but comparable to the corresponding standard deviations in the coupled model, suggesting that a major fraction of low-frequency local SAT variability over continents of the coupled model is generated in situ.

Over the continents of both the coupled and the mixed layer models, the spectral density of local SAT is nearly independent of frequency. On the other hand, the spectral density of local SAT over most of the oceans of both models increases very gradually with decreasing frequency apparently influenced by the thermal inertia of mixed layer oceans. However, both SST and SAT spectra in the coupled model are substantially different from those in the mixed layer model near the Denmark Strait and in some regions in the circumpolar ocean of the Southern Hemisphere where water mixes very deeply. In these regions, both SST and SAT are much more persistent in the coupled than in the mixed layer models, and their spectral densities are much larger at multidecadal and/or centennial timescales.

It appears significant that not only the coupled model but also the mixed layer model without ocean currents can approximately simulate the power spectrum of observed, global mean SAT at decadal to interdecadal timescales. However, neither model generates a sustained, long-term warming trend of significant magnitude such as that observed since the end of the last century.

1. Introduction

The time series of observed global mean surface air temperature (SAT), which have been compiled by various authors (e.g., Jones and Wigley 1991), exhibit temporal variability not only on the interannual but also on the decadal and interdecadal timescales. They also possess a slow but sustained global warming trend over the last 100-yr period.

One of the important processes that controls the unforced, low-frequency variation of sea surface temperature (SST) is the interaction between the oceans and the atmosphere. Hasselmann (1976) and Frankignoul and Hasselmann (1977) suggested that, in the midoceanic regions away from intense current and thermal fronts, the temporal variation of SST may be similar to a red noise response to random white noise thermal forcing from the atmosphere. It is expected that the spectrum of SST thus generated should in turn affect that of SAT. Since SST and SAT have more time for mutual adjustment at the lower frequency, the two spectra should become similar to each other, yielding a gradual increase of the SAT spectrum toward low frequency. We also speculate that this mechanism may be operating also over the continents. However, because of the small effective thermal inertia of the continental surface, the power spectra of both land surface temperature and SAT is almost white except at very short timescales, as will be shown later.

The temporal variation of ocean circulation could also be involved in very low frequency fluctuations of both SST and SAT. For example, Bjerknes (1964) speculated that interdecadal variations of SST in the

Corresponding author address: Dr. Syukuro Manabe, GFDL/NOAA, P.O. Box 308, Princeton, NJ 08542.
E-mail: sm@gfdl.gov

North Atlantic might result from fluctuations in the intensity of the thermohaline circulation. Recently, Kushnir (1994) detected a pattern of SST anomalies on the interdecadal timescale, which, in his speculation, is generated by temporal variations of the thermohaline circulation in the Atlantic Ocean. Analyzing a long-term integration of a coupled ocean–atmosphere model, Delworth et al. (1993) have shown that the coupled model can generate interdecadal variations of the thermohaline circulation in the North Atlantic Ocean and associated anomalies of SST that resemble the observed (Kushnir 1994).

Recently, Stouffer et al. (1994) extended the period of the above-mentioned integration of the coupled ocean–atmosphere model to 1000 years. They analyzed the temporal variation of the global mean SAT obtained from the coupled ocean–atmosphere model and compared it with the observed variation. Although the model does not yield a trend similar in magnitude and duration to the possibly anthropogenic warming trend of 0.5°C 110^{-1} yr observed since the end of the last century, it generates climate variability of interannual to interdecadal timescales comparable with observations.

The main goal of the present study is to acquire a global perspective on the role of oceans and continental surface in shaping the variability of climate. Extending the studies of Delworth et al. and Stouffer et al. mentioned above, it analyzes the variability and persistence of local and global mean SATs, which are obtained from a 1000-yr integration of the coupled atmosphere–ocean–land surface model, and compares them with available observations. It also explores how the temporal variation of local SAT is integrated to yield that of global mean SAT on interannual and longer timescales.

To identify the role of the oceans in the low-frequency fluctuation of climate, long-term integrations of three different models are performed and compared with each other. The first model, the "coupled model" described in section 2a, is constructed by combining a general circulation model of the atmosphere with that of oceans. The second model, the "mixed layer model" described in section 3a, is made by combining the general circulation model of the atmosphere with a very simple mixed layer ocean model in which the heat exchange between the mixed layer and deeper layer ocean is prescribed depending upon season and geography but does not change from one year to the next. By comparing long-term integrations of these two models, we hope to explore the role of the sub–mixed layer ocean and horizontal oceanic heat transport in determining the variability of climate. The third model, the "fixed SST model" described in section 3b, is the general circulation model of the atmosphere with observed SSTs, which vary with respect to season and geography. By comparing the integrations of the fixed SST with the coupled model, we hope to assess the influence of oceans, as a whole, upon the variability of climate.

2. Coupled model

a. Model structure

The coupled atmosphere–ocean–land surface model used in this study was developed for the study of global warming and is called coupled model for simplicity. The structure and performance of the model were described briefly by Stouffer et al. (1989) and in more detail by Manabe et al. (1991, 1992) and Manabe and Stouffer (1994). The model consists of a general circulation model of the global ocean coupled to a general circulation model of the atmosphere. Heat, water, and snow budgets at the continental surface are included. The model has global geography consistent with its computational resolution and seasonal (but not diurnal) variation of insolation.

In the atmospheric component of the model, dynamic computations are performed using the so-called spectral element method in which the distribution of a predicted variable is represented by a set of spherical harmonics (with 15 zonal waves and 15 associated Legendre functions) and grid values (Orszag 1970; Gordon and Stern 1982). There are nine unevenly spaced levels for the finite differencing in the vertical direction. The effects of clouds, water vapor, carbon dioxide, and ozone are included in the calculation of both solar and terrestrial radiation. Water vapor and precipitation are predicted in the model (Manabe et al. 1965), but a constant mixing ratio of carbon dioxide and a zonally uniform, seasonally varying, vertical distribution of ozone are prescribed. Overcast cloud is assumed whenever relative humidity exceeds a critical value (99%). Otherwise, clear sky is predicted.

The ocean model of Bryan and Lewis (1979) has been modified as described by Manabe et al. (1991). The finite-difference mesh used for the time integration of the primitive equations of motion has a spacing between grid points of 4.5° latitude and 3.7° longitude. It has 12 unevenly spaced levels in the vertical direction. In addition to the horizontal and vertical background subgrid-scale mixing and convective overturning, the model has isopycnal mixing as described by Redi (1982) and Tziperman and Bryan (1993). The model predicts sea ice using a simple model developed by Bryan (1969).

The atmospheric and oceanic components interact with each other through the exchanges of heat, water (including ice), and momentum at their interface. The water/ice flux includes runoff from the continents to the oceans. The runoff of meltwater from continental ice sheets, however, is not taken into consideration, assuming that the shapes of ice sheets are unchanged during the time integration of the coupled model.

b. Time integration

The initial conditions for the time integration of the coupled model have realistic seasonal and geographical distributions of surface temperature, surface salinity, and sea ice with which both the atmospheric and oceanic model states are nearly in equilibrium. When the time integration of the model starts from this initial condition, the model climate drifts toward its own equilibrium state, which differs from the initial condition described above. To reduce this drift, the fluxes of heat and water imposed at the oceanic surface of the coupled model are modified by the amounts that vary geographically and seasonally but do not change from one year to the next [see Manabe et al. (1991) and Manabe and Stouffer (1994) for details]. Since the adjustments are determined prior to the time integration of the coupled model and are not correlated to the transient anomalies of SST and SSS (i.e., sea surface salinity), which can develop during its integration, they are unlikely to either systematically amplify or dampen the anomalies. Owing to the flux adjustment technique described above, the model fluctuates around a realistic equilibrium state. One should also note, however, that this technique is quite different from the "restoring" that has been applied to SST and SSS during the time integration of an ocean-only model (e.g., Bryan and Cox 1967), which strongly damps surface anomalies.

Starting from the initial condition that was obtained and described above, the coupled model with the flux adjustments is integrated over a period of 1000 years. The mean trend in global mean surface air temperature during this period is very small and is -0.023°C century^{-1}. The trend of global mean temperature in the deeper layers of the model oceans is somewhat larger and is -0.07°C century^{-1}. This trend appears to result from the imperfection of the procedures that we developed for the determination of the initial condition and the time integration of the coupled model. The specific reasons for this trend, however, have not been identified and are under investigation.

3. Simpler models

a. Mixed layer model

Although the atmospheric and land surface components of this mixed layer model are identical to those of the coupled model described in section 2, its oceanic component is a simple mixed layer ocean model, which is a 50-m-thick slab of vertically well-mixed (but horizontally insulated) water. It contains a highly idealized scheme for sea ice prediction, which is identical to the thermodynamical part of the sea ice scheme used in the coupled model. With the exception of the prescribed heat flux described below, the model is similar to what was used by Manabe and Broccoli (1985) for their study of the climate of the last glacial maximum. The rate of heat exchange between the mixed layer and the deep ocean layers is prescribed such that the seasonal and geographical distributions of SST and sea ice thickness are realistic (Hansen et al. 1984). Again, one should note here that this prescribed heat flux is determined prior to the integration of the mixed layer model and is uncorrelated to the transient SST anomalies that develop during the course of the time integration of the mixed layer model. Therefore, it is not expected that the prescribed heat flux either amplifys or dampens the anomalies.

To determine the heat flux to be prescribed, a preliminary integration of the mixed layer model was performed over a period of 30 years starting from the initial condition of an isothermal atmosphere at rest. Throughout the course of this preliminary integration, SST and sea ice thickness are set to the observed climatological values. The heat required to maintain the observed values is averaged over 10 annual cycles between the twentieth and thirtieth years of this integration when the global mean surface air temperature of the model no longer changes systematically with time. In the integration of the mixed layer model described below, a seasonally and geographically varying heat flux is prescribed at the bottom of the mixed layer ocean such that it is equal to the heat source (or sink) computed here.

Starting from the state reached at the end of the preliminary integration, the mixed layer model was integrated over the period of 1000 years, allowing both the temperature and ice thickness of the mixed layer ocean to change thermodynamically. The heat flux, which was determined from the preliminary integration, was prescribed at the bottom of the mixed layer as a function of season and geography. Owing to this heat flux, no systematic drift of the model climate was indicated, and the geographical distributions of SST and sea ice thickness did not deviate significantly from the observed climatology.

b. Fixed SST model

This model also has the atmospheric and land surface components that are identical to those of the coupled model described in section 2. However, it has no oceanic component. Instead, SST is prescribed at observed climatological values that vary both geographically and seasonally. This model, called the fixed SST model, is integrated over a period of 500 years with very little trend.

c. Comparative analysis

As noted in the introduction, the climate variation obtained from the long-term integration of the coupled model described in section 2a is compared with the corresponding variations from the mixed layer and the fixed SST models to explore the role of the oceans in climate variability. Owing to the flux adjustments de-

scribed in section 2b, SST of the coupled model fluctuates around a realistic, seasonally varying temperature as noted already. Because of the heat flux prescribed at the bottom of the mixed layer ocean, the local SSTs of the mixed layer model do not drift systematically with time, again fluctuating around the realistic normals. The similarity of the time mean SSTs among the time integrations of the three models facilitates the comparable assessment of climate variabilities in these models.

To analyze, in the simplest possible way, the temporal variations of SAT at various timescales and their geographical distributions, the time series of local SST obtained from the three models are averaged over nonoverlapping but consecutive time intervals of 1, 5, and 25 years, removing most of the variations shorter than 2, 10, and 50 years, respectively. Three time series thus obtained are used to evaluate interannual and longer, decadal and longer, and one-half century and longer timescales, respectively. Obviously, it is desirable to select a sharply defined bandpass filter for the reliable analysis of SAT variability at different timescales. However, such a filter is not used in the present study in order to compare the simulated with the observed SAT variabilities. An observed SAT time series is usually too short to apply a spectrally well-defined filter, which requires many extra data points at both ends of the time series.

4. Surface air temperature

To examine geographically the natural variability of local SAT at various timescales, the standard deviations of annual, 5-, and 25-yr-mean SATs are illustrated (Figs. 1, 2, and 3) for the three models and are compared with the observations (Figs. 1a and 2a). Over the subtropical regions of the continents, both the coupled and mixed layer models overestimate the standard deviation of annual mean SAT anomalies, whereas they underestimate the anomalies in the eastern tropical Pacific Ocean (Fig. 1). With regard to the 5-yr-mean SAT anomalies, both models appear to overestimate it in the oceanic regions of low latitudes, particularly over the tropical Atlantic (Fig. 2). Except over these regions, both models simulate reasonably well the standard deviations of annual and 5-yr-mean SATs and their geographical distributions, with larger values over continents than over oceans. In all three models, the standard deviations of 5- and 25-yr-mean SATs are slightly less than one-half and one-quarter that of annual mean SAT, respectively. Exception to this occurs in some oceanic regions near the Antarctic Continent, in the Denmark Strait, and near the Sea of Okhotsk, where the standard deviation of time mean SAT of the coupled model decreases more gradually than other models as the period of averaging lengthens from 1 year to 25 years. It is also notable that the standard deviations over the continents of the fixed SST model for all three time

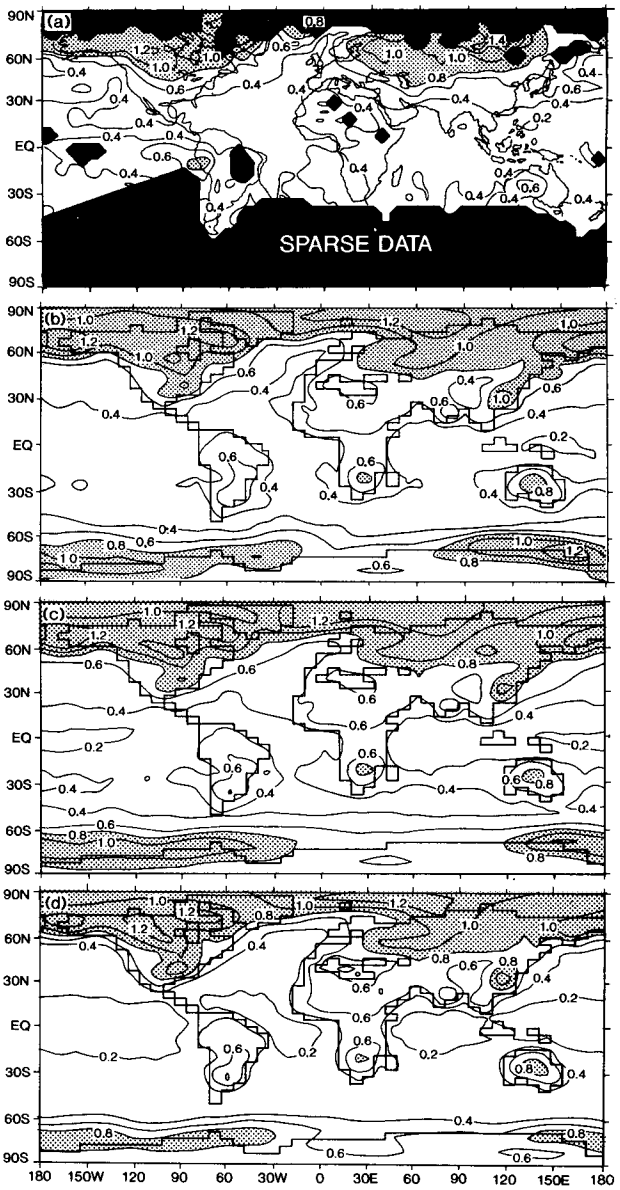

FIG. 1. Geographical distributions of the standard deviation of annual mean SAT anomaly (°C): (a) observed (Jones and Wigley 1991), (b) coupled model, (c) mixed layer model, (d) fixed SST model.

means are comparable to those from the other two models despite the absence of SST anomalies in the model.

To examine relative magnitudes of the standard deviations of the 5-yr-mean SAT from the three models, the geographical distributions of the ratios of standard deviation between the mixed layer model and the coupled model and between the fixed SST model and the coupled model are illustrated in Fig. 4. This figure indicates that the mixed layer model/coupled model ratio of the standard deviation of 5-yr-mean SAT is significantly less than one over the eastern tropical Pacific and immediate vicinities of the Antarctic Continent

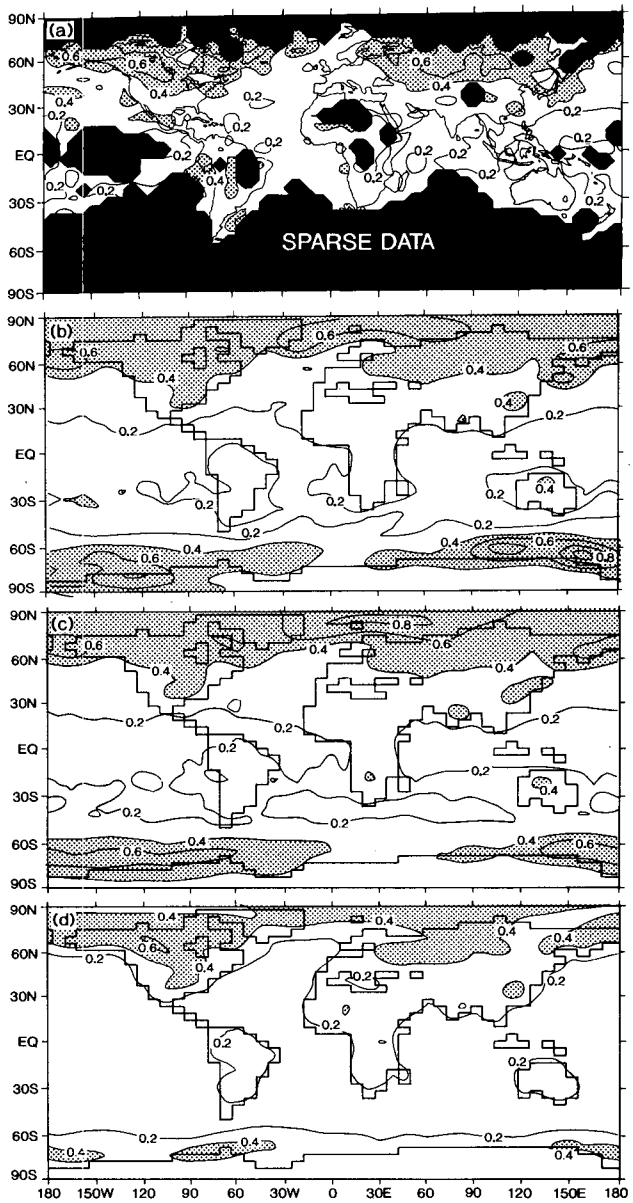

FIG. 2. Geographical distribution of the standard deviation of 5-yr-mean SAT anomaly (°C): (a) observed (Jones and Wigley 1991), (b) coupled model, (c) mixed layer model, (d) fixed SST model.

where the fluctuation of SST is enhanced due to the temporal variation of the thermal advection by ocean currents in the coupled model. On the other hand, the ratio is substantially larger than 1 over the belt stretching between the Davis Strait and Barents Sea, where the SAT variability is enhanced due to the fluctuation of sea ice coverage in winter, particularly in the mixed layer model. With the exception of these regions, the ratio is slightly larger than one, indicating that the SAT variability of the coupled model is slightly less than that of the mixed layer model over the continents and most of the oceans. This slight difference in the SAT variability is probably because the effective thermal inertia of oceans of the coupled model is slightly larger than that of the mixed layer model due to the heat exchange between the mixed layer and deeper layer of oceans.

The fixed SST model/coupled model ratio is less than 0.9 over Greenland, the northern boundary of Eurasia, and the Antarctic Continent. As discussed in section 5b, these regions are located near the oceanic regions of high latitudes where SST anomalies are relatively large and very persistent in the coupled model. However, over most of continental regions, the ratio is close to one.

The present analysis suggests that the coupled model generates in situ most of the decadal variability of SAT over continents with the exception of coastal regions located near the oceanic areas of persistent SST anomalies. The fixed SST model/coupled model ratio is also computed for the annual mean SAT (not shown). The regions where the ratio is less than 0.9 are even narrower, suggesting that the coupled model generates in

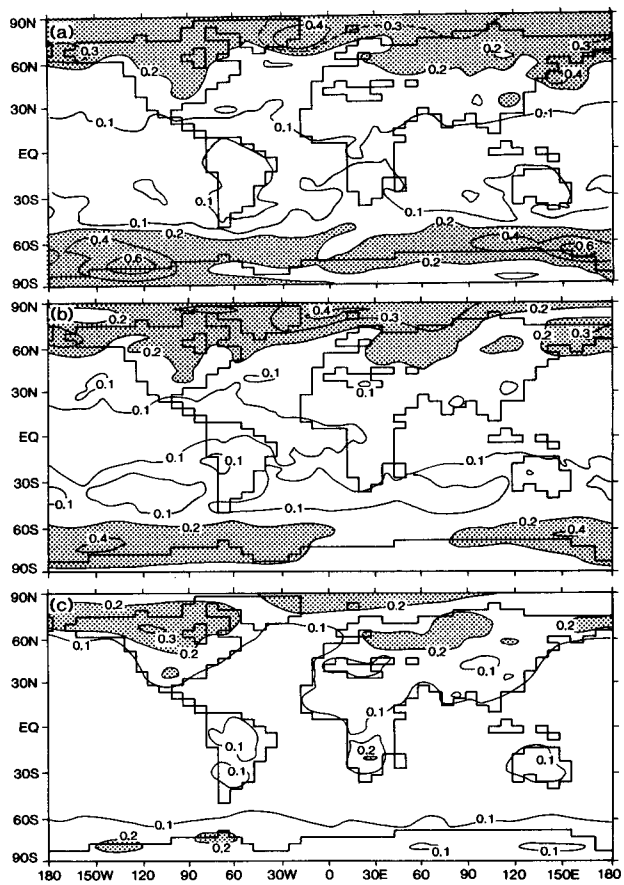

FIG. 3. Geographical distribution of the standard deviation of 25-yr-mean SAT anomaly (°C): (a) coupled model, (b) mixed layer model, (c) fixed SST model.

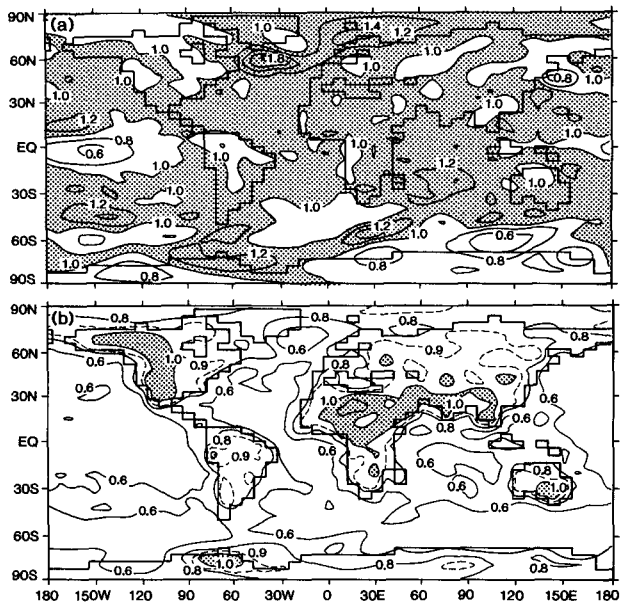

FIG. 4. Geographical distribution of the ratio of standard deviation of 5-yr-mean SAT anomaly: (a) mixed layer model/coupled model and (b) fixed SST model/coupled model. Contour interval is 0.2 with the exception of dashed line indicating 0.9 contour.

situ most of the interannual variability over the continents. Obviously, the present result does not exclude the possibility in which SST anomalies alter the spatial pattern of the principal modes over continents (e.g., Lau 1992) without significantly enhancing the magnitude of the atmospheric variability.

The interaction between the SAT anomalies over oceans and continents becomes more evident in Fig. 5, which compares two time series of annual mean SAT anomalies of the coupled model averaged over the entire continental and oceanic regions, respectively. This figure shows that, in contrast to local SAT, the globally averaged, continental and oceanic anomalies of annual mean SAT from the coupled model correlate well with each other. The correlation coefficient between the continental and oceanic SAT anomalies is 0.62, 0.74, and 0.82 for the 1-, 5-, and 25-yr-mean SAT, respectively, becoming larger with increasing period of averaging. In short, the interaction between the SAT anomalies over continents and oceans becomes more evident as the spacial and temporal scales of the anomalies increase. Although this statement appears to be contradictory to the suggestion that most of the SAT variability over continents are generated in situ, it is not so. As a matter of fact, the variance of continentally averaged SAT anomaly is much less than the continentally averaged variance of local SAT anomaly. The ratio between these two quantities turned out to be 0.047, 0.067, and 0.083 for the 1-, 5-, and 25-yr-mean SAT, respectively. This result implies that, over continents, there exist ample low-frequency variabilities of local

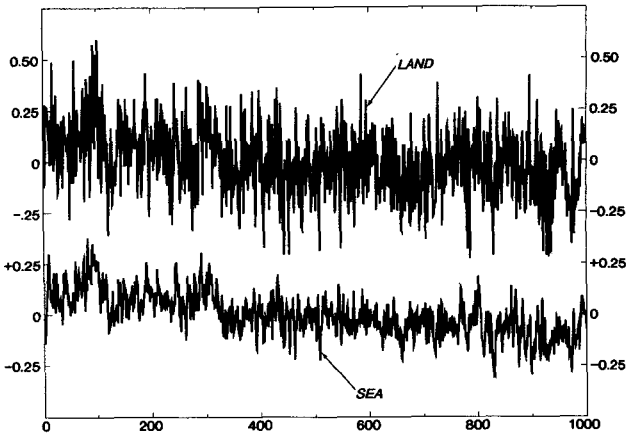

FIG. 5. Time series of SAT anomalies averaged over the entire continental and oceanic regions. Upper and lower lines represent continental and oceanic time series, respectively.

SAT that are not correlated to either continental- or oceanic-scale anomalies.

Figure 6 illustrates, for the coupled model, the area-averaged spectra of local SAT anomalies over the wide continental and oceanic zonal belt located between 30° and 60°N. It shows that, over the continental belt, the spectra of local SAT anomalies are essentially white, resulting in the approximate halving of SAT standard deviation as the averaging period increases from 1 to 5 years or 5 to 25 years. The spectral density, however,

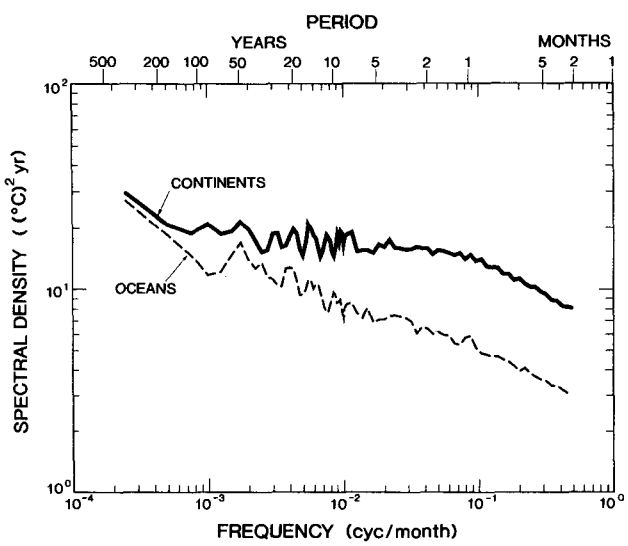

FIG. 6. Power spectra of monthly mean SAT anomaly of the coupled model. Continental and oceanic spectra are obtained by averaging the spectra of all grid points, which are located inside the 30°–60° latitude belt in the Northern Hemisphere, respectively. The spectra are the smoothed Fourier transform of the autocovariance function using a Tukey window with a maximum of 2400 (200 years) lags. They are smoothed by the equally weighted averaging over the logarithmic (base 10) interval of 0.04 in frequency.

decreases very slightly with increasing frequency beyond 1 cycle per year. Over oceans, it decreases gradually with increasing frequency as influenced by the thermal inertia of the underlying oceans. Thus, the spectral density over continents is larger than over oceans, particularly at high frequencies, where the thermal inertia of oceans effectively reduces the magnitude of anomalies.

To examine the persistence of local SAT anomalies, lag-one autocorrelations are computed for the time series of 1- and 5-yr-mean SAT obtained from the 1000-yr integration of the coupled model (Fig. 7). This figure indicates that the lag-one autocorrelation is relatively large over certain oceanic regions in high latitudes. Of special interest are the regions of persistence in the Pacific and Indian Ocean sectors of the circumpolar ocean of the Southern Hemisphere, where the lag-one autocorrelation is hardly reduced as the period of SAT averaging increases from 1 to 5 years and to 25 years (not shown). As described in the following section, SST anomalies in these regions of the coupled model exhibit centennial timescale variations, accounting for the persistence of the time mean SATs described above. In the Northern Hemisphere, the SAT anomalies of the coupled model are particularly persistent around the Denmark Strait and near the Sea of Okhotsk, again being influenced by the persistent SST anomalies. In middle and low latitudes, the lag-one autocorrelation coefficient has small positive values for annual mean SAT anomalies, but area mean coefficients approach zero as the period of averaging increases from 1 to 5 years and 25 years (not shown).

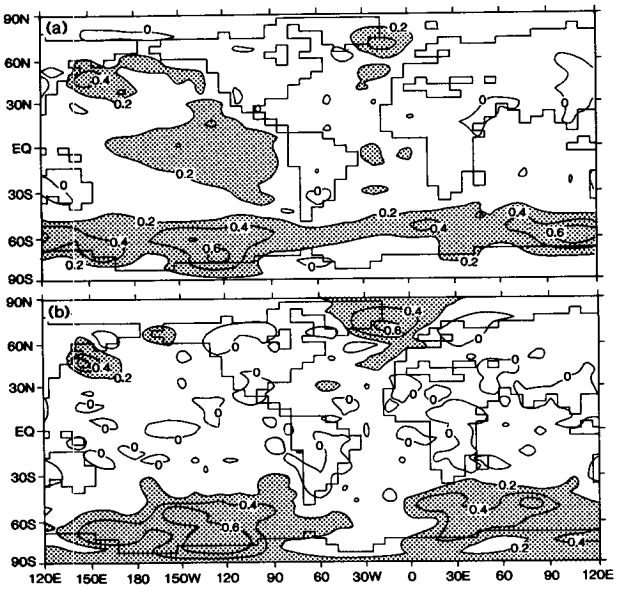

FIG. 7. Geographical distribution of lag-one autocorrelation coefficient of (a) annual mean SAT and (b) 5-yr-mean SAT anomalies of the coupled model.

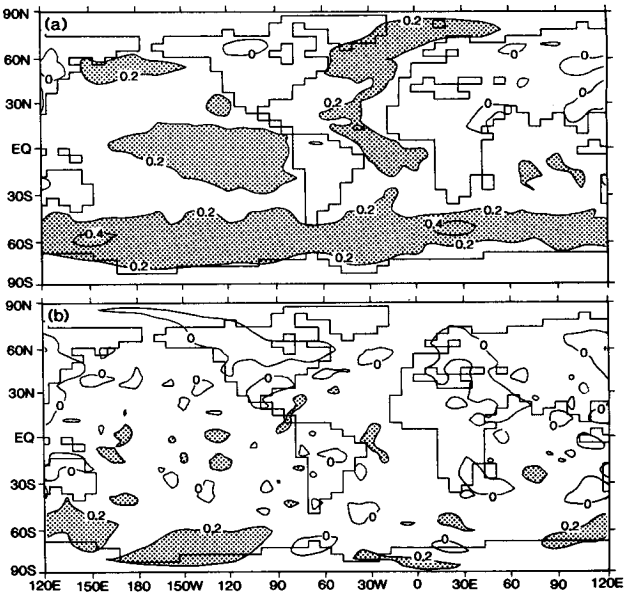

FIG. 8. Geographical distribution of lag-one autocorrelation coefficient of (a) annual mean SAT and (b) 5-yr-mean SAT anomalies of the mixed layer model.

The geographical distributions of the lag-one autocorrelation coefficients are also computed for the mixed layer model and are illustrated in Fig. 8. The autocorrelation pattern of 1-yr-mean SAT anomaly (Fig. 8a) resembles the corresponding pattern of the coupled model (Fig. 7a). For example, due to the positive feedback effect involving sea ice in the mixed layer model, the autocorrelation coefficient is relatively large in the northern North Atlantic and over the circumpolar ocean of the Southern Hemisphere. In certain regions of these oceans, the coefficients are, however, smaller in magnitude than in the coupled model. As discussed in the following section, deep oceanic circulation and associated convection make SSTs very persistent in these regions of the coupled model. As the averaging period of SAT increases from 1 to 5 years (Fig. 8b), the autocorrelation coefficient decreases markedly in these regions of the mixed layer model in sharp contrast to the situation of the coupled model. Although the autocorrelation coefficients of the annual mean SAT anomalies are relatively large in the eastern tropical Pacific of both mixed layer and coupled models, they become small as the averaging period of SAT increases from 1 year to 5 years. Further analysis of the interannual variations of SAT anomalies in the eastern tropical Pacific of both models is in progress.

5. Sea surface temperature

a. Variability and persistence

As discussed in the introduction, the mutual adjustment between SAT and SST anomalies are more com-

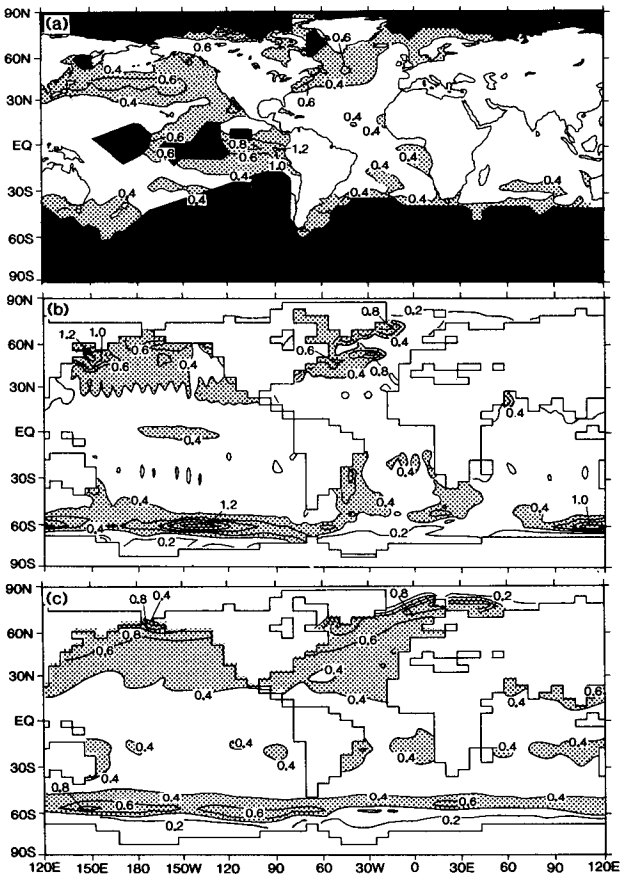

FIG. 9. Geographical distribution of the standard deviation of annual mean SST anomaly: (a) observed (Bottomley et al. 1990), (b) coupled model, (c) mixed layer model.

plete at low frequencies (i.e., decadal and longer timescales). This section describes and discusses the temporal variation of SST and its effect on SAT in the coupled and mixed layer models.

The standard deviations of annual mean SST anomalies in the coupled and mixed layer models are computed and their geographical distributions are compared with the values derived from observed SSTs compiled by Bottomley et al. (1990) (Fig. 9). In qualitative agreement with observations, the variability of annual mean SST of the coupled model is relatively large in the northwestern portion of the North Atlantic. The standard deviation of SST anomaly from the coupled model is also large in the Pacific sector of the circumpolar ocean of the Southern Hemisphere where the SST observations are very sparse. It is encouraging, however, that the standard deviation of observed SST anomaly tends to increase toward the circumpolar ocean. Although one notes a belt of weak local maximum of SST standard deviation in the central equatorial Pacific, it is much less pronounced than the wide belt of large standard deviation that stretches over the eastern half of the tropical Pacific in the observed distribution. As noted by Lau et al. (1992) and Knutson and Manabe (1994), the coupled model generates a phenomenon that resembles the Southern Oscillation. However, because of the coarse computational resolution of the model, the amplitude of the oscillation is much less than the observed, accounting for the failure of the model to generate a realistic magnitude of standard deviation in the eastern tropical Pacific.

With the exception of certain regions in the circumpolar ocean of the Southern Hemisphere and the northern North Atlantic and northwestern North Pacific, the standard deviation of annual mean SST in the mixed layer model is slightly larger than the coupled model. The damping of SST anomalies by oceanic advection and subgrid-scale mixing is missing in the mixed layer model, accounting for the slight difference in the standard deviation of SST anomalies between the two models.

To evaluate the persistence of SST anomaly, lag-one autocorrelations of annual mean SST time series are computed for both coupled and mixed layer models and

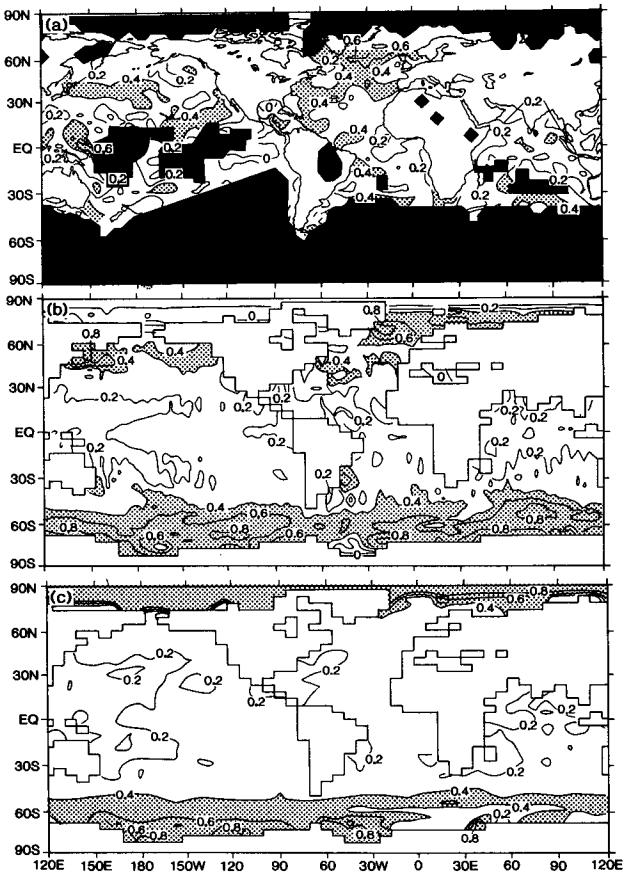

FIG. 10. Geographical distribution of lag-one autocorrelation coefficient of annual mean SST anomaly: (a) observed (Bottomley et al. 1990), (b) coupled model, (c) mixed layer model.

their geographical distributions are compared with the observations (Fig. 10). In general, the persistence of SST anomalies of the coupled model is relatively small in low latitudes where the evaporative damping of the anomalies predominates. It increases with increasing latitudes in qualitative agreement with observations. The persistence is pronounced in the circumpolar ocean of the Southern Hemisphere, around the Denmark Strait, and near the Sea of Okhotsk where the anomalies of 5- and 25-yr-mean SAT are also very persistent (section 4). As the static stability of ocean decreases from the low to the high latitudes of the coupled model, oceanic circulation and associated convection deepen, contributing to the latitudinal dependence of persistence described above. In the mixed layer model in which the effect of thermal advection by ocean currents is absent, the latitudinal increase of the persistence is much less evident than the coupled model. It is of interest, however, that the SST anomalies are also persistent near the Antarctic Continent and the Denmark Strait of the mixed layer model as influenced by the positive sea ice albedo feedback.

With the exception of the region near the Sea of Okhotsk, the regions of large persistence of SST anomaly in the coupled model are situated in the neighborhood of those oceanic regions where the greenhouse warming penetrates very deeply in a numerical experiment conducted by Manabe et al. (1991). Figure 17a of their paper illustrates geographically the effective penetration depth of temperature anomaly when the concentration of atmospheric CO_2, increasing at the compounded rate of 1% per year, doubles. It indicates that the downward penetration of temperature anomaly is particularly deep in the circumpolar ocean of the Southern Hemisphere and in the region to the south of Greenland. As noted earlier, annual mean SST anomalies in the 1000-yr integration of the coupled model are also very persistent in those regions, where oceanic circulation and associated convection penetrate very deeply. Thus, the thermal advection by slowly varying, deep circulation is responsible for the persistence of SST anomalies of the coupled model as discussed in the following section 5b.

b. *Power spectra*

As noted in the introduction, Hasselmann (1976) proposed his theory of the mixed layer ocean to explain the observed SST spectrum. He expressed the prognostic equation of SST anomaly T by

$$C\frac{dT}{dt} = f_w - \gamma T, \tag{1}$$

where C is the effective heat capacity of mixed layer ocean, f_w is the thermal forcing of oceans by the atmosphere, which he characterized as white noise, and γ is the rate of thermal damping. Based upon Eq. (1), he suggested that the observed SST variation may be characterized as a red noise response of the mixed layer ocean to white noise forcing from above as represented by

$$G(\omega) = \frac{(F_0/C)^2}{(\gamma/C)^2 + \omega^2}, \tag{2}$$

where $G(\omega)$ is the spectral density of SST response, ω is angular frequency, and F_0 is power of the white noise forcing. As noted by Hasselmann, the spectrum of the atmospheric forcing may be regarded as almost white at the timescales that are much longer than the duration of a typical atmospheric disturbance.

To examine whether the variabilities of local SST anomalies of the coupled and mixed layer models are consistent with the stochastic theory of Hasselmann's, power spectra of monthly mean SST anomalies obtained from the two models are averaged over both the central North Pacific and central North Atlantic and are illustrated in Fig. 11. For reference, the least square fit of Eq. (2) to the SST spectrum of the coupled model is also indicated by a thin line. This figure clearly indicates that, in the midoceanic regions, the SST spectra of both models may be characterized as red noise spectra represented by Eq. 2. It also indicates that, despite the absence of large-scale circulation, the midoceanic spectrum of the mixed layer model is similar in magnitude to that of the coupled model.

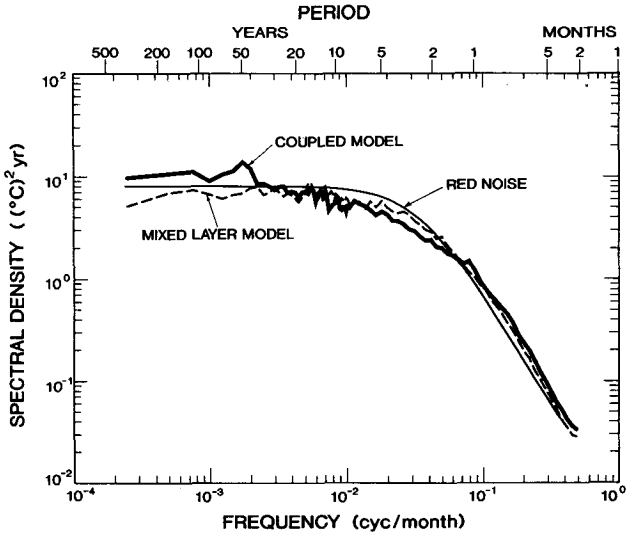

FIG. 11. Power spectra of monthly mean SST anomaly of the coupled (thick solid line) and the mixed layer (dashed line) models. Both spectra are obtained by averaging the spectra of all grid points, which are located in the midoceanic boxes of the North Pacific (42.2°–28.9°N, 155.6°E–140.1°W) and North Atlantic (42.2°–28.9°N, 61.9°E–28.1°W). The spectra are the smoothed Fourier transform of the autocovariance function using a Tukey window with a maximum of 2400 (200 years) lags. They are smoothed by the equally weighted averaging over the logarithmic (base 10) interval of 0.04 in frequency. The red noise spectrum represented by a thin line is the least square fit of Eq. (2) to the spectrum of SST from the coupled model.

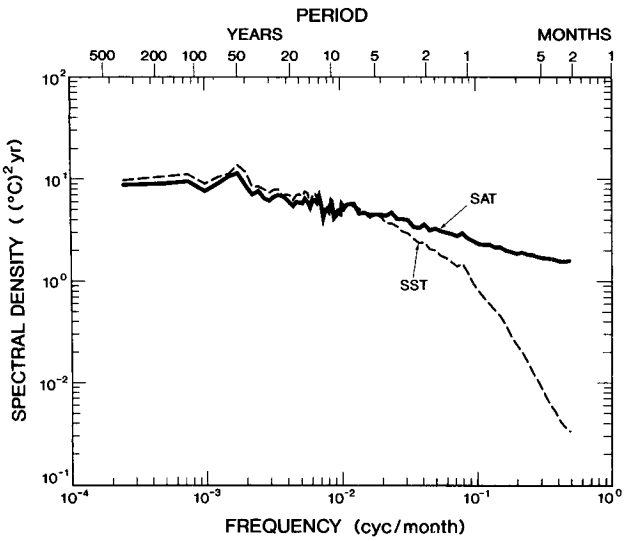

FIG. 12. Power spectra of monthly mean SST (dashed line) and SAT (solid line) anomalies of the coupled model. Both spectra are obtained by averaging the spectra of all grid points, which are located in the midoceanic boxes of the North Pacific (42.2°–28.9°N, 155.6°E–140°W) and North Atlantic (42.2°–28.9°N, 61.9°E–28.1°W). The spectra are the smoothed Fourier transform of the autocovariance function using a Tukey window with a maximum of 2400 (200 years) lags. They are smoothed by the equally weighted averaging over the logarithmic (base 10) interval of 0.04 in frequency.

In Fig. 12, the area-mean spectrum of monthly mean SST anomalies, computed for the midoceanic box of the coupled model, is compared with the corresponding spectrum of monthly mean SAT anomalies. This comparison reveals that these two spectra are very similar at low frequencies beyond 1 cycle for every few years. However, the power of the SST spectrum is much smaller than that of the SAT spectrum at high frequencies. This is because the thermal inertia of oceans suppresses significantly the high-frequency fluctuation of SAT generated by the cyclone wave activities in the atmosphere. On the other hand, at low frequencies, SAT anomalies over the oceans have enough time to fully adjust to large SST anomalies through boundary layer heat exchange, accounting for the similarity between SST and SAT spectra at these frequencies.

The stochastic theory of Hasselmann could also be used to evaluate the area-mean spectrum of local SAT anomalies over continents shown in Fig. 6. However, the effective heat capacity of continental surface, as determined by the penetration depth of temperature anomalies in soil, is much less than that of oceans. When heat capacity C in Eq. (2) is small, the response spectrum of SST $G(\omega)$ may be approximated by

$$G(\omega) \approx (F_0/\gamma)^2. \qquad (3)$$

Thus, at most frequencies, the continental surface temperature is in equilibrium with the white noise thermal forcing from the atmosphere, yielding a white noise power spectrum. Since the effective thermal inertias of both continental surface and atmospheric boundary layer are small, SAT and surface temperature have enough time to adjust to each other, yielding almost white noise spectra of similar magnitudes at timescales longer than a few months (Fig. 6).

As noted already, the mean power spectrum of local SAT anomalies over continents, however, decreases slightly with increasing frequency beyond 1 cycle yr^{-1}. Delworth and Manabe (1989, 1993) have shown that the temporal variation of soil moisture may also be characterized as the red noise response to the white noise forcing of the difference between precipitation and evaporation. The soil moisture variation, in turn, affects the relative magnitudes of sensible and latent heat fluxes, which remove the radiative energy absorbed by the continental surface. Thus, the temporal variation of sensible heat flux, and accordingly that of the thermal forcing of continental surface, are enhanced at seasonal and longer timescales, contributing to the slight bending of the SAT spectrum at the high frequencies.

In contrast to the situation over the midoceanic regions described earlier, the spectrum of SST anomaly near the Denmark Strait, which are obtained from both coupled and mixed layer models, deviate significantly from the red noise spectrum and have a very distinct peak at 1 cycle yr^{-1} (Fig. 13), reflecting the large year-to-year fluctuations of winter sea ice coverage and SAT anomaly in the region. One also notes that the spectral density of SST anomaly from the coupled model is

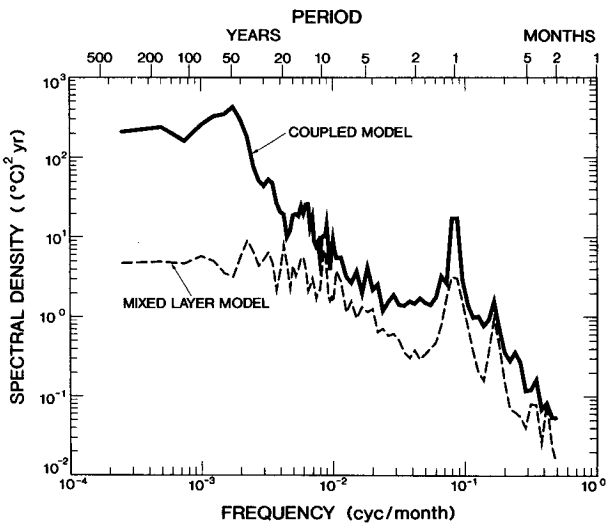

FIG. 13. Power spectra of monthly mean SST anomaly at 69.75°N, 22.5°W of the coupled (solid line) and the mixed layer (dashed line) models. The spectra are the smoothed Fourier transforms of autocovariance function using a Tukey window with a maximum of 2400 (200 years) lags. They are smoothed by the equally weighted averaging over the logarithmic (base 10) interval of 0.04 in frequency.

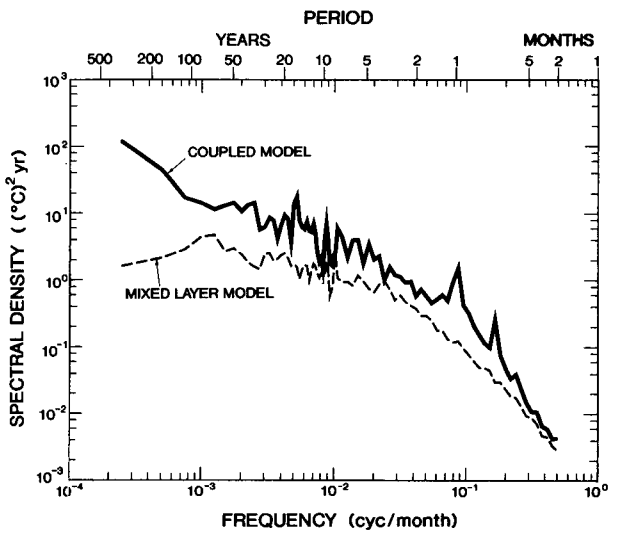

FIG. 14. Power spectra of monthly mean SST anomaly at 60.75°S, 142.5°W of the coupled (solid line) and the mixed layer (dashed line) models. The spectra are the smoothed Fourier transforms of autocovariance function using a Tukey window with a maximum of 2400 (200 years) lags. They are smoothed by the equally weighted averaging over the logarithmic (base 10) interval of 0.04 in frequency.

much larger than the mixed layer model at the frequencies lower than 1 cycle $(30\ \text{yr})^{-1}$ and has a moderate peak at around 1 cycle $(50\ \text{yr})^{-1}$ (Fig. 13). Such a peak is missing in the corresponding power spectrum obtained from the mixed layer model (Fig. 13), suggesting that the SST fluctuation associated with the spectral peak mentioned above is induced by the temporal variation of ocean circulation in the coupled model. A preliminary analysis indicates that this SST fluctuation near the Denmark Strait results from the temporal variation in the southward advection of SST by the East Greenland Currents as a part of a meridionally overturning cell. The fluctuation of this cell, in turn, appears to be associated with the irregular oscillation of the North Atlantic thermohaline circulation, which also has the timescale of about 50 years and was identified by Delworth et al. (1993) in the 1000-yr integration of the coupled model. The pattern of the SST anomaly generated by the oscillation resembles what Kushnir (1994) obtained from the observations.

The "teleconnection" between the temporal variation of SST in the Denmark Strait and that of SAT in the surrounding regions is examined by computing the correlation coefficient between the two. The teleconnection pattern thus obtained (not shown) indicates that the low-frequency fluctuation of SST near the Denmark Strait influences SATs not only in the northern North Atlantic but also in the Scandinavian Peninsula and western Europe.

In the Pacific sector of circumpolar ocean of the Southern Hemisphere, the SST anomaly of the coupled model is large and persistent as noted already. The power spectrum representing its temporal variation is significantly different from the red noise spectrum represented by Eq. (2), with largest spectral density at lowest frequency. Figure 14 compares the power spectra of SST between the coupled and mixed layer models at 60.75°S and 142.5°W of the circumpolar ocean, where the standard deviation of SST anomaly is at a maximum in the coupled model. This comparison indicates that, at this location, the spectral density of SST is larger in the coupled than the mixed layer model. The difference between the two spectra is small at high frequencies, increases with decreasing frequency, and becomes large at centennial timescales. To inspect more directly the SST variation of the coupled model, the time series of the annual mean SST at this location is obtained from the 1000-yr integration of the coupled model and is illustrated in Fig. 15 together with its 25-yr running mean. This figure shows that the SST of the coupled model exhibits large variations over multicentury timescales. This centennial fluctuation is superposed by an equally large fluctuation of decadal timescales with the exception of the period between the ~70th and ~230th year when the sea surface is relatively warm and almost free of winter sea ice. Although it is not shown here, sea surface salinity (SSS) also fluctuates in phase with temperature at both multicentennial and decadal timescales. The decadal fluctuations of both SST and SSS described above appear to result from intermittent convection induced by the freezing of sea ice and associated brine formation. On the other hand, the longer multicentennial fluctuations of both SST and SSS appear to be associated with the very gradual change of deep circulation which, in turn, induces the centennial excursions of both SST and SAT by affecting the northward advection of cold and fresh surface layer in the circumpolar ocean of the Southern Hemisphere. An in-depth analysis of the low-frequency variability in the circumpolar ocean is in progress.

We have shown that the coupled model generates very persistent SST anomalies in certain regions of sub-

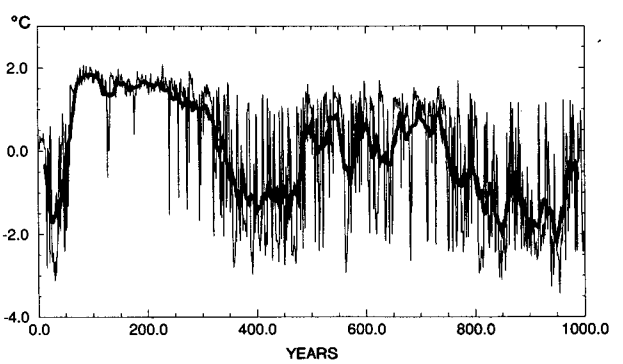

FIG. 15. 1000-year time series of annual mean SST anomaly (thin line) with its 25-yr running mean (thick line) at 60.75°S, 142.5°W of the coupled model.

polar oceans. In certain selected regions of the circumpolar ocean of the Southern Hemisphere, the state of oceanic surface alternates on centennial timescales between the warm and cold periods associated with changes in deep circulation. In the North Atlantic, the temporal variation of thermohaline circulation induces SST anomalies with the timescale of about one-half century (Delworth et al. 1993). However, large abrupt changes of the North Atlantic climate and associated fluctuations of the thermohaline circulation such as Alleröd–Younger Dryas transition and Dansgaad–Oeschger events (e.g., Broecker 1990) did not occur in the 1000-yr integration of the coupled ocean–atmosphere model. This model behavior appears to be consistent with the absence of large, abrupt climate changes as shown by the time series of isotopic temperature obtained from the Greenland Ice Cores during the Holocene (GRIP 1993). It is important to note, however, a major fluctuation of the thermohaline circulation did occur in the North Atlantic of the coupled model in response to the doubling of the atmospheric concentration of CO_2 (Manabe and Stouffer 1994). Because of the capping of oceanic surface by relatively fresh water resulting from the large CO_2-induced increase of precipitation in high latitudes, the thermohaline circulation in the North Atlantic of the coupled model weakened by a factor of 2 or more and became shallower, thereby reducing the rate of deep water formation. However, it regains the original intensity by the end of the 500-yr experiment. The weakening and reintensification of the thermohaline circulation and the pattern of the associated change in SST resemble the paleoceanographic signature of Younger Dryas events as described, for example, by Keigwin and Lehman (1994). Despite the absence of massive ice sheets, which could yield large amount of meltwater, the supply of fresh water into the Arctic and North Atlantic Oceans could increase markedly resulting from the global warming. Therefore, one should not eliminate the possibility that a major fluctuation of the thermohaline circulation could occur in the North Atlantic in response to the future increase of greenhouse gases in the atmosphere.

6. Global mean temperature

The detection of global warming has been an important goal of climate research. It is, therefore, useful to assess whether the observed warming of about 0.5°C over the last 110 years is attributable to the increase of thermal forcing such as the increase of greenhouse gases or the natural variation of climate resulting from the interaction among the atmosphere, oceans, and land surface. For this purpose, the time series of global mean SAT anomalies from the 1000-yr integrations of the coupled and mixed layer models are compared with the time series of observed SAT in Fig. 16. This figure shows that both model time series have very small trends that are −0.023°C and 0.011°C per century, respectively, and are much less than the observed trend, which is about 0.52°C century^{-1}. It also indicates the standard deviations of global mean SAT anomalies from both models are similar at annual to interdecadal timescales. Although there are periods during which the rate of warming is as large as 0.5°C century^{-1} in both model time series, these periods appear to last only a few decades.

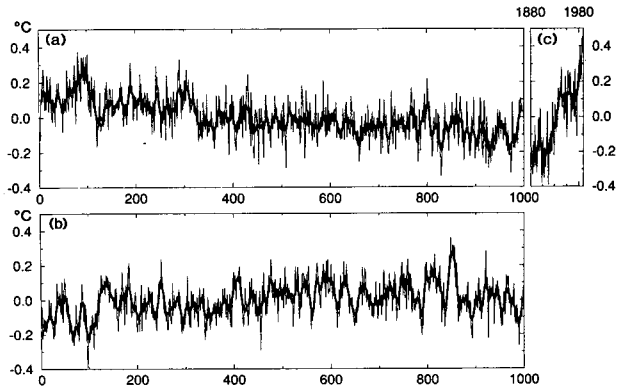

FIG. 16. Time series of globally averaged, annual mean SAT (°C) anomaly from the long-term mean: (a) 1000-yr time series from the coupled model, (b) 1000-yr time series from the mixed layer model, (c) 110-yr (1881–1990) time series of observed globally averaged SAT compiled by Jones and Wigley (1991). Note that 10-yr running mean curves are added to all time series.

To assess the probability of finding a century-scale warming trend such as that observed between 1881 and 1990 in the 1000-yr time series of global mean SAT from the coupled model, Stouffer et al. (1994) calculated the probability for linear trends exceeding 0.5°C century^{-1}. They found that, for intervals longer than ~60 yr, there are no trends as large as 0.5°C century^{-1}. In other words, the observed warming trend of 0.52°C century^{-1} is not found in the coupled model time series for any intervals longer than ~60 yr. Essentially similar results are obtained for the time series from the mixed layer model. In short, it is not very likely that the ocean–atmosphere interaction in either the coupled or the mixed layer model could randomly generate a substantial long-term warming trend, such as that observed since the end of the last century.

To examine spectrally the temporal variation of global mean SAT anomaly shown in Fig. 16, the power spectra of detrended and globally averaged monthly mean SAT anomalies from the 1000-yr integrations of both coupled and mixed layer models are compared in Fig. 17 with the spectrum of detrended, observed SAT compiled by Jones and Wigley (1991). The detrending of the observed time series removes most of the contributions from the fluctuation on a timescale longer than 100 years. At interdecadal or shorter timescales, the spectra from both models are not very different from the observed spectrum, although the estimates of both models are lower than observed over the interval

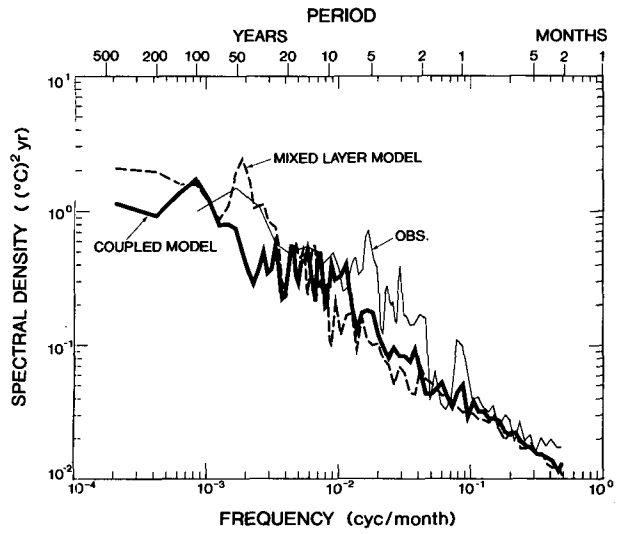

FIG. 17. Power spectra of detrended globally averaged, monthly mean SAT anomaly. The solid line represents the coupled model; the dashed line represents the mixed layer model (to detrend the time series, the least square method is used); the thin solid line represents observed [obtained by use of the data compiled by Jones and Wigley (1991)]. The spectra are the smoothed Fourier transforms of autocovariance function using a Tukey window with a maximum of 2400 (200 years) lags for the models and 480 (40 years) lags for the observed. They are smoothed by the equally weighted averaging over the logarithmic (base 10) interval of 0.04 in frequency.

from 1 to 10 years. As noted by Lau et al. (1992) and Knutson and Manabe (1994), a low-resolution coupled ocean–atmosphere model underestimates substantially the magnitude of the Southern Oscillation, resulting in the underestimation of spectral power at interannual timescales.

Figure 17 also indicates that the power spectrum of global mean SAT anomaly from the mixed layer model is similar to the coupled model spectrum. Despite the existence of interdecadal to centennial oscillation in certain high latitude regions of the coupled model, the spectral resemblance suggests that similar physical mechanisms may be playing a dominating role in shaping the global mean SAT spectra of the two models. In short, the mixed layer model appears to mimic more or less the low-frequency variability of global mean SAT in the coupled model despite the absence of ocean circulation.

To distinguish the global warming due to greenhouse gases from the internally generated variation of climate, it is desirable to know the pattern of internal variation of SAT associated with a given change of global mean SAT. Figures 18b and 18c illustrate the geographical distribution of the regression coefficient of 5-yr-mean SAT on its global mean value obtained from the 1000-yr integrations of the coupled and the mixed layer models. (Here, the regression coefficient indicates the change of local SAT which accompanies a 1°C increase in the global mean SAT.) The regression pattern of the observed 5-yr-mean SAT is also added for comparison. These figures indicate that, in both coupled and mixed layer models, the regression coefficients are relatively large over the Eurasian and North American continents. The coefficients have smaller positive values over most of the oceanic regions. Qualitatively similar features are indicated in the regression pattern of the observed SAT, though the Eurasian maximum is not as pronounced. In view of the fact that the standard deviation of 5-yr-mean SAT anomalies of both coupled and mixed layer models are larger over continents than over oceans in Fig. 2, it is reasonable that the SAT anomalies over both Eurasian and North American continents tend to be large when the global mean SAT is high. It is notable that not only the regression pattern but also the power spectrum of global mean SAT is similar between the two models as noted earlier. The similarity appears to imply that the thermal advection by ocean circulation plays a secondary role in determining the variability of global mean SAT.

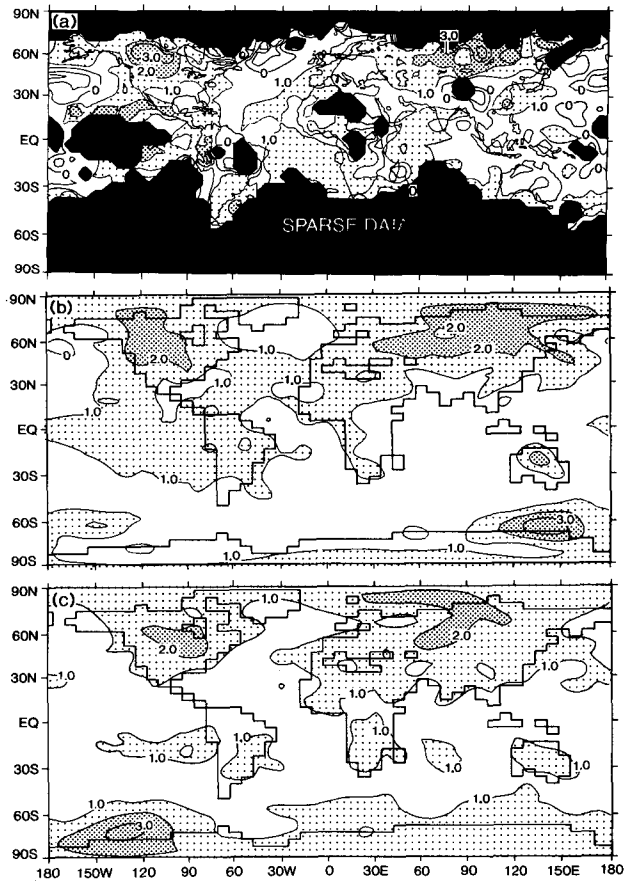

FIG. 18. Geographical distributions of regression coefficient of local, 5-yr-mean SAT anomaly on the globally averaged, 5-yr-mean SAT: (a) observed (Jones and Wigley 1991), (b) the coupled model, (c) the mixed layer model. The regression coefficient obtained here indicates the slope of a line which least square fits the plots of local vs globally averaged, 5-yr-mean SAT anomalies at each grid point.

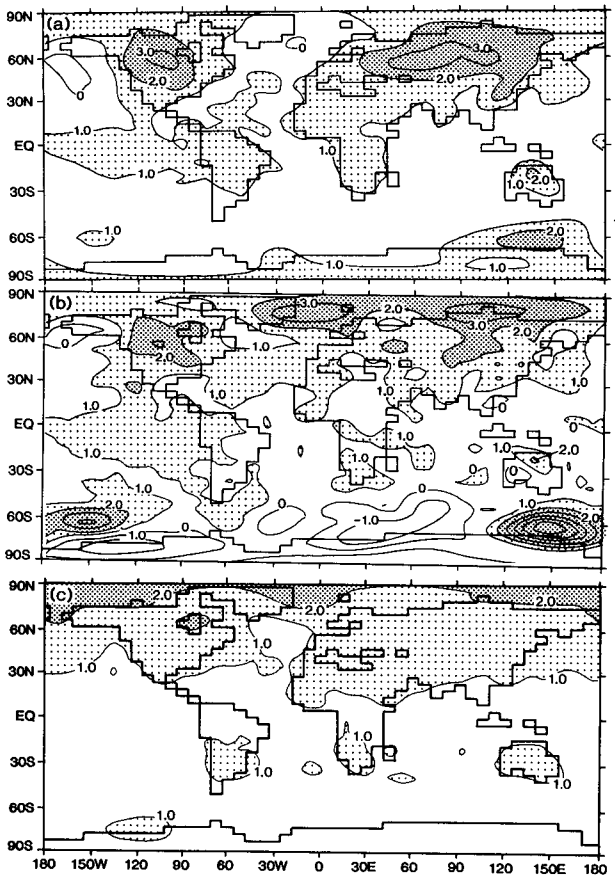

FIG. 19. Geographical distributions of (a) the coefficient of regression of local, annual mean SAT on globally averaged annual mean SAT anomalies, (b) the coefficient of regression of local, 25-yr-mean SAT on globally averaged, 25-yr-mean SAT anomalies, and (c) the normalized change in SAT of the coupled model in response to the gradual increase of the atmospheric CO_2. The normalized SAT change is constructed by averaging the SAT change over the 61st–80th-year period of the experiment when the CO_2 concentration is approximately doubled and dividing it by its global mean value. This figure (c) is almost identical to Fig. 13b of the paper by Manabe et al. (1991) except that the experiment started from slightly different initial conditions.

The regression patterns are computed not only for 5-yr-mean SAT but also for 1- and 25-yr-mean SATs of the coupled model (Figs. 19a and 19b). These patterns may be compared with the pattern of the CO_2-induced change of the coupled model SAT, which is normalized by its global mean value (Fig. 19c). [The CO_2-induced change of SAT shown here was obtained by Manabe et al. (1991) as the transient response of the coupled model to a gradual increase, that is, 1% per year compounded, of the atmospheric CO_2.] By comparing Fig. 19c with Figs. 19a and 19b, one can evaluate whether the fingerprint of the CO_2-induced warming is different from the warming associated with the internally generated variation of climate. For example, the CO_2-induced warming is larger over continents than over oceans where the effective thermal inertia is larger and evaporative damping of SST anomalies is stronger as discussed by Manabe et al. (1991). The land–sea contrast in the warming, however, is even more pronounced in the pattern of the internally generated warming with small regions of slight cooling in the northern North Atlantic and North Pacific Oceans. The slight cooling in these regions appear to result from the enhanced southward advection of cold air in the coupled model's atmosphere. On the other hand, the relatively small CO_2-induced SAT increase in the northern North Atlantic is attributable to not only the deep vertical mixing of water but also the reduction in the northward advection of warm surface water by the thermohaline circulation (Manabe et al. 1991). It is also notable that the CO_2-induced warming has significant polar amplification due to the enhanced heat conduction through thinner sea ice (Manabe and Stouffer 1979, 1980), whereas the regression pattern of annual mean SAT indicates a local minimum over the Arctic Ocean.

We have noted, however, that the pattern of regression coefficient (of local on global mean SAT anomalies) changes as the averaging period of SAT increases from 1 year (Fig. 19a) to 5 years (Fig. 18b) and 25 years (Fig. 19b). For example, the regression pattern of local on global 25-yr-mean SAT anomalies have the smallest land–sea contrast with some tendency toward polar amplification with local maximums around the Denmark Strait and Taymyr Peninsula. This may be consistent with the studies of Vinnikov et al. (1979, 1982) and Kelly et al. (1982), which detected a polar amplification in the temporal variation of observed, zonal mean SAT with interdecadal and longer timescales. In view of the fact that the similar feature is missing in the regression pattern of 25-yr-mean SAT from the mixed layer model (not shown), this polar amplification may not result from the thinning of sea ice, but from the low-frequency oscillation of thermohaline circulation in the North Atlantic discussed earlier. Despite some notable differences, there is the broad-scale similarity between the pattern of the CO_2-induced and the internally generated warming at multidecadal timescales, making it difficult to distinguish between the two types of warming.

7. Summary and concluding remarks

It has been shown that, with the exception of the tropical Pacific, both coupled and mixed layer models simulate reasonably well the observed variability of local SAT at interannual and decadal timescales. The simulated variability is usually larger over continents than over oceans in agreement with observations. This land–sea contrast in variability holds not only for the annual but also for the decadal and multidecadal timescales.

The spectrum of monthly mean SAT over continents is almost white with slight downward bend at the fre-

quencies higher than 1 cycle yr^{-1}. The power of the SAT spectrum over most of oceans, however, increases very gradually with decreasing frequency as influenced by the thermal inertia of underlying oceans, and approaches the power of the continental spectrum at decadal and longer timescales. In other words, local variabilities of SAT over continents are larger than those over oceans not only at interannual but also at decadal and longer timescales. We believe that this difference results mainly from the smaller evaporative damping of surface temperature anomaly over continents as compared with oceans.

It is found that, in the midoceanic regions of the middle latitudes, the spectrum of SST anomalies of both coupled and mixed layer models may be characterized as a red noise spectrum indicative of a first-order Markov process. This result appears to be consistent with the stochastic theory of Hasselmann, which regards the observed variation of SST anomaly as the red noise response to the random white noise forcing from the atmosphere. (At timescales that are sufficiently longer than the decay timescale of an atmospheric disturbance, the spectrum of atmospheric forcing may be regarded as white.) The red noise SST anomalies, in turn, affect SAT anomalies, resulting in the aforementioned, gradual increase of spectral power with decreasing frequencies.

Hasselmann's theory can also be applied to evaluate the temporal variation of continental surface temperature. Since the effective thermal inertia of continental surface is small, the surface temperature is in equilibrium with the almost–white noise thermal forcing from the atmosphere, yielding a white noise power spectrum with the exception of very short timescales. The white noise fluctuation of surface temperature, in turn, closely interacts with the atmosphere mainly through boundary layer heat exchange, maintaining the almost–white noise spectrum of SAT as described above. It is notable that, over most of the continental regions, the standard deviation of SAT anomalies of the fixed SST model is comparable to that of the coupled model not only at interannual but also decadal timescales. This result suggests that the coupled model generates in situ a major fraction of low-frequency SAT variation over continents. However, it does not exclude the possibility that the SST anomalies over oceans alter the low-frequency variation of SAT over continents. As a matter of fact, the decadal SAT variability of the coupled model appears to be enhanced in some continental areas located near the subpolar regions of oceans where SST anomalies are relatively large and persistent. If the Southern Oscillation of the coupled model were larger and more realistic, SST anomalies in the Tropics could also have enhanced SAT variability over continents.

The interaction between the SAT anomalies over continents and oceans becomes more evident as the spacial as well as temporal scales of anomalies increase. For example, the low-frequency variabilities of SAT averaged over the entire continental regions and over the entire oceanic regions are well correlated with each other. The low-frequency variability of the local SAT, however, is much larger than the variability of SAT anomaly averaged over the entire continental regions.

The applicability of the stochastic theory is reduced in certain subpolar regions of oceans where oceanic circulation and associated convection often penetrate very deeply. These regions include the Greenland–Iceland–Norwegian (GIN) sea and the circumpolar ocean of the Southern Hemisphere. In these regions, both SST and SAT are very persistent and their spectral densities at decadal and longer timescales are much larger in the coupled than the mixed layer model, as influenced by the advection by low-frequency ocean circulation and associated convective activity. For example, the multidecadal fluctuation of SST near the Denmark Strait results from the fluctuation of the East Greenland Current, which may, in turn, be associated with the multidecadal oscillation of thermohaline circulation in the North Atlantic recently analyzed by Delworth et al. (1993). In certain regions of the circumpolar ocean of the Southern Hemisphere, the state of oceanic surface alternates on centennial timescales between warm and cold periods, associated with the fluctuation of deep circulation. This centennial fluctuation is superposed by equally large SST fluctuations on decadal timescales, which tend to be pronounced during the cold period because of brine formation resulting from the freezing of sea ice. The very low-frequency variations of SST in the GIN sea and circumpolar ocean of the coupled model are described in section 5b and are the subjects of in-depth analysis in the near future.

In a global warming experiment, which was conducted recently with the coupled model (Manabe et al. 1991), it was found that the response of SST to the increase of atmospheric CO_2 is very small in those subpolar regions where the timescale of natural variability is very long. Because of deep vertical mixing of water, the effective thermal inertia of ocean is very large in the northern North Atlantic and circumpolar ocean of the Southern Hemisphere and is responsible for the large delay in the global warming mentioned above.

Since the late nineteenth century, the global mean surface air temperature has increased at the rate of about 0.5°C $century^{-1}$ (IPCC 1990). Stouffer et al. (1994) tried to find such a long-term trend in the 1000-yr time series of the global mean SAT obtained from the integration of the coupled model. They found that, during the entire time series, a temperature trend as large as 0.5°C $century^{-1}$ was never sustained over the period longer than 60 years. A similar statement is also valid for the 1000-yr time series obtained from the mixed layer model (see also Davies and Hunt 1994). Assuming that the low-frequency variability of the coupled model is realistic, these results suggest that the observed trend is not caused by the interaction among

the atmosphere, ocean, and continental surface. Instead, it may have been induced by a sustained trend in thermal forcing such as solar irradiance, atmospheric greenhouse gas, and aerosol loading.

Wigley and Raper (1990) discussed the response of global mean surface temperature to the atmospheric forcing using a simple "zero dimensional" atmospheric model coupled with an "upwelling diffusion" oceanic model. They noted that the amplitude of global mean temperature fluctuation is inversely proportional to the coefficient of effective radiative damping (i.e., the feedback parameter), which determines the sensitivity of global temperature to a thermal forcing. The equilibrium response of the global mean surface air temperature of the coupled model to the doubling of atmospheric CO_2 has been estimated to be 3.5°C (Manabe and Stouffer 1994), which is in the upper half of the 1.5°–4.5°C range obtained by the Intergovernmental Panel on Climate Change. A model with smaller sensitivity would have smaller variability than this coupled model, making it less likely to yield an internally generated long-term trend similar to the observed warming of the past 100 years.

Despite the failure of both coupled and mixed layer models to generate trends on centennial timescales similar to that observed since the end of the last century, they approximately reproduce the power spectrum of observed global mean SAT at decadal and interdecadal timescales. It is also notable that the global mean SAT spectra from the coupled and mixed layer models are similar to each other: the powers of both spectra increase almost monotonically with decreasing frequency. However, the spectral density of local SAT is almost white over continents and decreases very gradually with increasing frequency over oceans, and is quite different from global mean SAT spectrum described above. The difference between the spectra of local and global mean SAT suggests that, at high frequencies, SAT anomalies tend to have relatively small scales and hardly contribute to the variability of the global mean SAT. On the other hand, SAT anomalies with very low frequency tend to have almost global scale, which includes both oceans and continents, and contribute more effectively to the variability of the global mean SAT. Thus, the spectral densities of global mean SAT of both coupled and mixed layer models decreases substantially with increasing frequency at interdecadal and shorter timescales despite almost white noise–like behavior of local SAT anomalies. Although there are large and persistent anomalies of both SST and SAT near the Denmark Strait and the circumpolar ocean of the Southern Hemisphere, their contributions are not large enough to make the power spectrum of global mean SAT of the coupled model significantly different from that of the mixed layer model.

Since both models approximately simulate the observed power spectrum of global mean SAT at decadal and interdecadal timescales as noted above, one is tempted to speculate that the observed variation of SAT at these timescales is attributable solely to the interaction among the atmosphere, oceans, and land surface. However, the spectral similarity does not necessarily exclude the possibility that the temporal variation of various thermal forcings such as solar irradiance and volcanic aerosols in the stratosphere (Hansen et al. 1984) could also contribute in comparable magnitude to the fluctuation of observed global mean SAT at these timescales.

To distinguish the climate change resulting from the increase of greenhouse gases and other thermal forcings from the internally generated climate variability due to the interaction among the atmosphere, ocean, and land surface, it is desirable to know whether the pattern of the former differs significantly from the pattern of the latter. To explore this issue, we compared the horizontal distribution of the normalized, CO_2-induced SAT change with the coefficient of regression between the global mean and local SAT anomalies in the 1000-yr integration of the coupled model. Despite some notable differences, broad scale similarity is indicated between the two patterns with larger warming over the continents as compared with the oceans. Therefore, it may be difficult to detect the greenhouse warming by use of a pattern recognition technique, which involves SAT as noted, for example, by Wigley and Jones (1981). One should note, however, that the pattern of the anthropogenic change of climate would be different from what is shown in Fig. 19c if the negative thermal forcing of sulphate aerosols were taken into consideration in addition to the positive CO_2 forcing (e.g., Charlson et al. 1992; Taylor and Penner 1994). Because of the increased reflection of the insolation by the anthropogenic sulphate particles over continents and their immediate vicinities, the land–sea contrast in the anthropogenic warming may have been reduced (Mitchell et al. 1995), thereby making it more distinguishable from the internally generated warming with larger land–sea contrast (for further discussion of this topic, see, for example, Santer et al. 1995). Obviously, it is very urgent to monitor the thermal forcing of both natural and man-made aerosols to distinguish the anthropogenic from the internally generated warming.

In addition to the experiments discussed in this study, several multiple century integrations of the models similar to the coupled and mixed layer models used here have been performed recently at the Max Planck Institute of Germany, the Hadley Center of England, the CSIRO of Australia (Davies and Hunt 1994), and the Center for Ocean–Land–Atmosphere Studies of the United States (Schneider and Kinter 1994). The comparative assessment of the SAT variability in some of these models is being conducted by the 1995 Intergovernmental Panel of Climate Change.

In assessing the results from the present study, one should recognize that the coupled model used here has

relatively low computational resolution and fails to resolve explicitly mesoscale eddies in oceans (see section 2a). Thus, it fails to generate SST fluctuations of realistic magnitude with a seasonal timescale. Although the coupled model can simulate a phenomenon that resembles the Southern Oscillation (Knutson and Manabe 1994), the amplitude of the oscillation is only one-third as large as the observed, grossly underestimating the SST variability of interannual timescale in the tropical oceans. As noted by Philander et al. (1992), higher computational resolution may be required in order to generate a realistic Southern Oscillation. It is also likely that the relatively large subgrid-scale mixing coefficient associated with the poor computational resolution of the present coupled model may damp too strongly the SST anomalies. We are encouraged, however, that the coupled model approximately reproduces the standard deviations of annual and 5-yr-mean SAT anomalies and their geographical distributions with the important exception of the eastern tropical Pacific. Currently, a long-term integration of a coupled model with higher computational resolution and smaller coefficients of subgrid-scale mixing is in progress, yielding a more realistic amplitude of the Southern Oscillation. The analysis of the difference between the low- and high-resolution model experiments should be useful for reassessing the results obtained from the present study.

Acknowledgments. We thank Thomas Delworth who contributed to the analysis of the relationship between the North Atlantic thermohaline circulation and SST anomaly in GIN sea (section 5). He, Isaac Held, N.-C. Lau, Stephen Griffies, Jerry Mahlman, and Alan Robock have given us many comments that were very useful for the improvement of the manuscript. We are grateful to Jerry Mahlman, the Director of GFDL, who wholeheartedly supported this project and approved the usage of massive computer resources needed for many long-term integrations of the coupled ocean–atmosphere model.

REFERENCES

Bjerknes, J., 1964: Atlantic air–sea interaction. *Adv. Geophys.*, **10,** 1–82.

Bottomley, M., C. K. Folland, J. Hsiung, R. E. Newell, and D. E. Parker, 1990: Global ocean surface temperature atlas (GOSTA). Joint Meteorological Office/Massachusetts Institute of Technology Project supported by U.S. Department of Energy, U.S. National Science Foundation, and U.S. Office of Naval Research, Her Majesty's Stationary Office, London, 20 + iv pp. and 313 plates.

Broecker, W. S., 1990: Massive iceberg discharges as triggers for global climate change. *Nature,* **372,** 421–424.

Bryan, K., 1969: Climate and the ocean circulation. Part II: The ocean model. *Mon. Wea. Rev.,* **97,** 806–827.

——, and M. D. Cox, 1967: A numerical integration of the oceanic general circulation. *Tellus,* **19,** 54–80.

——, and L. J. Lewis, 1979: A water mass model of the world ocean. *J. Geophys. Res.,* **84**(C5), 2503–2517.

Charlson, R. J., S. E. Schwarz, J. M. Hales, R. D. Cess, J. A. Coakley Jr., J. E. Hansen, and D. J. Hofmann, 1992: Climate forcing by anthropogenic aerosols. *Science,* **255,** 423–430.

Davies, H. L., and B. G. Hunt, 1994: The problem of detecting climate change in the presence of climatic variability. *J. Meteor. Soc. Japan,* **72,** 765–771.

Delworth, T., and S. Manabe, 1989: The influence of soil wetness on near-surface atmospheric variability. *J. Climate,* **2,** 1447–1462.

——, and ——, 1993: Climate variability and land surface processes. *Adv. Water Resour.,* **16,** 3–20.

——, ——, and R. J. Stouffer, 1993: Interdecadal variation of the thermohaline circulation in a coupled ocean–atmosphere model. *J. Climate,* **6,** 1993–2011.

Frankignoul, C., and K. Hasselmann, 1977: Stochastic climate models. Part II: Application to sea-surface temperature anomalies and thermohaline variability. *Tellus,* **29,** 289–305.

Gordon, C. T., and W. Stern, 1982: A description of the GFDL Global Spectral Model. *Mon. Wea. Rev.,* **110,** 625–644.

GRIP (Greenland Ice-Core Project) Members, 1993: Climate instability during the last interglacial period recorded in the GRIP ice core. *Nature,* **364,** 203–207.

Hansen, J., A. Lacis, D. Rind, G. Russel, and P. Stone, 1984: *Climate Sensitivity. Geophys. Monogr.,* No. 29, Maurice Ewing, Vol. 5, J. E. Hansen and T. Takahashi, Eds., Amer. Geophys. Union, 130–163.

Hasselmann, K., 1976: Stochastic climate models. Part I: Theory. *Tellus,* **28,** 473–485.

IPCC (Intergovernmental Panel on Climate Change), 1990: *Scientific Assessment of Climate Change.* WMO-UNEP, Cambridge University Press, 366 pp.

Jones, P., and T. M. L. Wigley, 1991: Global and hemispheric anomalies. *Trend '91: A Compendium of Data on Global Change,* T. A. Boden, R. J. Sepanski, F. W. Stoss, Eds., Oak Ridge National Laboratory, 512–517.

Keigwin, L. D., and S. J. Lehman, 1994: Deep circulation change linked to Heinrich event 1 and Younger Dryas in a middepth North Atlantic core. *Paleoceanography,* **9,** 185–194.

Kelly, P. M., P. D. Jones, C. B. Sear, B. S. G. Cherry, and R. K. Tavakol, 1982: Variation in surface air temperature. Part 2: Arctic regions, 1881–1980. *Mon. Wea. Rev.,* **110,** 71–83.

Knutson, T. R., and S. Manabe, 1994: Impact of increased CO_2 on simulated ENSO-like phenomena. *Geophys. Res. Lett.,* **21,** 2295–2298.

Kushnir, Y., 1994: Interdecadal variation in North Atlantic sea surface temperature and associated atmospheric condition. *J. Climate,* **7,** 141–157.

Lau, N. C., 1992: Climate variability simulated in GCMs. *Climate System Modeling,* K. E. Trenberth, Ed., Cambridge University Press, 617–642.

——, S. G. H. Philander, and M. J. Nath, 1992: Simulation of ENSO-like phenomena with a low-resolution coupled GCM of the global ocean and atmosphere. *J. Climate,* **5,** 284–307.

Manabe, S., and R. J. Stouffer, 1979: A CO_2-climate sensitivity study with a mathematical model of the global climate. *Nature,* **282,** 491–493.

——, and R. J. Stouffer, 1980: Sensitivity of a global climate model to an increase of CO_2 concentration in the atmosphere. *J. Geophys. Res.,* **85**(C10), 5529–5554.

——, and A. J. Broccoli, 1985: A comparison of climate model sensitivity with data from the last glacial maximum. *J. Atmos. Sci.,* **42,** 2643–2651.

——, and R. J. Stouffer, 1994: Multiple-century response of a coupled ocean–atmosphere model to an increase of atmospheric carbon dioxide. *J. Climate,* **7,** 5–23.

——, J. Smagorinsky, and R. F. Strickler, 1965: Simulated climatology of a general circulation model with a hydrologic cycle. *Mon. Wea. Rev.,* **93,** 769–798.

——, R. J. Stouffer, M. J. Spelman, and K. Bryan, 1991: Transient response of a coupled ocean–atmosphere model to gradual changes of atmospheric CO_2. Part I: Annual mean response. *J. Climate,* **4,** 785–818.

——, M. J. Spelman, and R. J. Stouffer, 1992: Transient response of a coupled ocean–atmosphere model to gradual changes of atmospheric CO_2. Part II: Seasonal response. *J. Climate,* **5,** 105–126.

Mitchell, J. F. B., T. C. Jones, J. M. Gregory, and S. F. B. Tett, 1995: Climate response to enhanced greenhouse gases and sulphate aerosols. *Nature,* **376,** 501–504.

Orszag, S. A., 1970: Transform method for calculating vector-coupled sums: Application to the spectral form of the vorticity equation. *J. Atmos. Sci.,* **27,** 890–895.

Philander, S. G. H., R. C. Pacanowski, N.-C. Lau, and M. J. Nath, 1992: Simulation of ENSO with a global atmospheric GCM coupled to a high resolution tropical Pacific Ocean GCM. *J. Climate,* **5,** 308–329.

Redi, M. H., 1982: Oceanic isopycnal mixing by coordinate rotation. *J. Phys. Oceanogr.,* **12,** 1154–1158.

Schneider, E. K., and J. L. Kinter III, 1994: An examination of internally generated variability in long climate simulations. *Climate Dyn.,* **10,** 181–204.

Stouffer, R. J., S. Manabe, and K. Bryan, 1989: Interhemispheric asymmetry in climate response to a gradual increase of atmospheric CO_2. *Nature,* **342,** 660–662.

——, ——, and K. Y. Vinnikov, 1994: Model assessment of the role of natural variability in recent global warming. *Nature,* **367,** 634–636.

Taylor, K. E., and J. E. Penner, 1994: Anthropogenic aerosols and climate change. *Nature,* **369,** 734–736.

Tziperman, E., and K. Bryan, 1993: Estimating global air–sea fluxes from surface properties and from climatological flux data using an oceanic general circulation model. *J. Geophys. Res.,* **98**(C12), 22 629–22 644.

Vinnikov, K. Y., and P. Y. Groisman, 1979: Empirical model of modern climate changes. *Meteor. Gidrol.,* **3,** 25–36.

——, and ——, 1982: The empirical study of climate sensitivity. *Izvestiya, Acad. Sci., USSR Atmos. Oceanic Phys.,* **18**(11), 895–902.

Wigley, T. M. L., and P. Jones, 1981: Detecting CO_2-induced climate change. *Nature,* **292,** 205–208.

——, and S. C. B. Raper, 1990: Natural variability of the climate system and detection of the greenhouse effect. *Nature,* **344,** 324–327.